Orbital-Angular-Momentum Polarization Mode Dispersion in Optical Fibers

Lixian Wang, Pravin Vaity, Stéphane Chatigny, Younés Messaddeq, Leslie A. Rusch, and Sophie LaRochelle

Journal of Lightwave Technology, (Volume 34, Issue 8) (2016)

Doi: 10.1109/JLT.2015.2506461

http://ieeexplore.ieee.org/document/7348637/?arnumber=7348637&tag=1

This article has been accepted for publication in a future issue of this journal, but has not been fully edited. Content may change prior to final publication. Citation information: DOI 10.1109/JLT.2015.2506461, Journal of Lightwave Technology

Orbital-Angular-Momentum Polarization Mode Dispersion in Optical Fibers

Lixian Wang[1], Pravin Vaity[1], Stéphane Chatigny[2], Younés Messaddeq[1], Leslie A. Rusch[1], *Fellow, IEEE* and Sophie LaRochelle[1], *Senior member, IEEE, Fellow, OSA*

(*Invited Paper*)

***Abstract*— The orbital-angular-momentum (OAM) modes in optical fibers have polarization-mode dispersion (PMD) properties similar to those of single mode fibers (SMFs). The +*l* and –*l* order OAM modes supported by the same fiber vector modes undergo random cross-coupling and exhibit a frequency dependent time delay. We name this effect "OAM-PMD" and extend the formalism developed for PMD in SMFs to describe OAM-PMD. The characteristics of the modal beat lengths, birefringence correlation lengths and the mean-value of OAM-PMD are investigated. A fixed-analyzer technique is proposed and demonstrated to characterize this phenomenon in OAM fibers. Two different types of OAM fiber are examined. The measured results are compared with the theoretical calculations.**

***Index Terms*—optical fibers, optical fiber polarization, optical fiber communication, optical fiber testing**

I. Introduction

ORBITAL angular momentum (OAM) of light is associated with the helical phase front proportional to exp(*ilφ*) where *l* is the topological charge (*l*=0, ±1, ±2, …) and *φ* is the azimuthal angle [1]. The orthogonal OAM mode set provides a new degree of freedom to increase the optical communication capacity in addition to other freedoms that have already been widely used such as the wavelength, time and polarization [2]. OAM-division multiplexing have been demonstrated in both optical free-space [3]–[5] and fiber optic communications [6].

Optical fiber that can support stable transmission of OAM modes is the key component in OAM-based fiber optical communication systems. Generally, in cylindrical optical fibers, a linear combination of the degenerate even and odd HE (EH) vector modes has a helical phase front, i.e. carrying OAM. The existence of near-degeneracy of the vector modes inside a given mode group would cause strong mode coupling and consequently make OAM modes unstable during propagation. As in the case of polarization-maintaining fibers (PMFs), the first step for stabilizing OAM modes in fibers is to lift the mode degeneracy [7].

A variety of OAM fibers have been proposed with either solid [8]–[10] or hollow cores [11], [12]. Most of them feature a ring-shaped refractive index profile and a large index contrast between the core and cladding. A properly designed OAM fiber should provide a large separation of the effective indices between the adjacent EH and HE modes (Δn_{eff}>10^{-4}), which is a phenomenological rule that favors the stable propagation of the orthogonal polarizations of the LP_{01} modes in conventional PMFs [13].

Ideally the even and odd HE (EH) modes that constitute an OAM mode should have the same propagation constant, *i.e.* no walk-off, so that the OAM mode maintains its mode profile and topological charge. Fiber imperfections such as core ellipticity and internal stress, and external perturbations, such as twists and bends, can induce δn_{eff} between the nominally degenerate even and odd vector modes, namely the modal birefringence. Note that δn_{eff} represents the modal birefringence while Δn_{eff} is the effective index separation between the modes of the unperturbed fiber design. The modal birefringence together with a random variation of the birefringence orientation would give rise to a random coupling between +*l* and -*l* order OAM states during propagation. This effect is similar to polarization mode dispersion (PMD) in single mode fibers (SMFs). We call it "OAM-PMD".

The impact of an elliptical core on the modal birefringence was simulated in [14] and the birefringence-induced deterioration of the OAM DeMUX efficiency was investigated. However the authors did not consider the random variation of the orientation of the modal birefringence. In an experimental demonstration of OAM-division multiplexing [6], a polarization controller was inserted at the transmitter end of each OAM channel to compensate for the OAM-PMD, but the OAM-PMD was not discussed in detail.

Recently Antonelli *et al.* generalized the concept of PMD to mode dispersion (MD) in multimode fibers [15]. A MD vector was defined in a D-dimensional extended Stokes space. When there is mode coupling, the MD vector undertakes a D-dimensional isotropic random walk. In OAM fibers, the situation could be largely simplified. This is because the vector modes are separated in the effective index space and they rarely couple to each other over a relatively long length of fiber. Therefore, each vector mode in an OAM fiber can be described separately in its own 3D Stokes space in a similar way as that for SMFs. Starting from this idea, we extend in this paper the formalism developed for PMD in SMFs. In section II, we discuss the polarization states of OAM modes in fibers and

[1]Lixian Wang, Pravin Vaity, Younés Messadeqq, Leslie Rusch and Sophie LaRochelle are with Centre d'optique, photonique et laser (COPL), Université Laval, Québec, QC, Canada, G1V 0A6. (e-mail: Sophie.larochelle@gel.ulaval.ca.

[2]Stéphane Chatigny is with the CorActive High-Tech Inc., Québec, QC, Canada, G2C 1S9. (e-mail: Stephane.Chatigny@coractive.com).

This article has been accepted for publication in a future issue of this journal, but has not been fully edited. Content may change prior to final publication. Citation information: DOI 10.1109/JLT.2015.2506461, Journal of Lightwave Technology

their representation on the Poincaré sphere. In section III, we develop an OAM-PMD model based on the concatenation of fixed-birefringence fiber sections with random orientation (well-known fixed birefringence model). In section IV, a fixed-analyzer technique is then proposed and demonstrated to measure the mean value of OAM-PMD in OAM fibers. Two different types of OAM fibers designed and fabricated in our lab are tested and compared for various orders of OAM-modes. We also present through numerical simulations and measurements an investigation of the local birefringence of both fibers. This is followed, in section V, by a discussion comparing theoretical predictions and experimental results. This paper is a full-length extension of our recent publication in European Conference on Optical Communications (ECOC 2015) [16].

II. Polarization States of OAM Modes in Optical Fibers

In cylindrical optical fibers, the solution of the Maxwell's vector wave equations is a set of vector modes, *i.e.* HE, EH, TE and TM modes. Fig. 1 (a) to (d) shows a few examples of the states of polarization (SOPs) of vector modes. Their electrical fields are spirally polarized, analogous to the so-called vectorial vortex (VV) beams in free space [17] (the SOP of the fundamental HE_{11} mode is spatially homogeneous but it can be considered as the 0-order VV). At each point on the cross section of a vector mode, the orientation angle θ of the electrical field (with respect to the x-axis of the (x, y) coordinate system as shown in Fig. 1 (f)) is a function of the azimuthal angle ϕ:

$$\theta=\begin{cases}-|l|\phi & \mathrm{HE}_{|l|+1,m}\ \text{even}\\ -|l|\phi+\pi/2 & \mathrm{HE}_{|l|+1,m}\ \text{odd}\\ |l|\phi & \mathrm{EH}_{|l|-1,m}\ \text{even and TE}_{01}\ (|l|=1)\\ |l|\phi+\pi/2 & \mathrm{EH}_{|l|-1,m}\ \text{odd and TM}_{01}\ (|l|=1)\end{cases} \tag{1}$$

where l=0, ±1, ±2, ±3… is the topological charge indicating the order of OAM that a vector mode can support and m is the radial order. If we define a local Cartesian coordinate system (x', y') in which the angle between the x'-axis and the x-axis equals the azimuthal angle ϕ in (x, y) coordinate system (Fig. 1 (f)), the local orientation angle θ', defined as the angle between the modal electrical and the x'-axis, can be expressed as:

$$\theta'=\begin{cases}-(|l|+1)\phi & \mathrm{HE}_{|l|+1,m}\ \text{even}\\ -(|l|+1)\phi+\pi/2 & \mathrm{HE}_{|l|+1,m}\ \text{odd}\\ (|l|-1)\phi & \mathrm{EH}_{|l|-1,m}\ \text{even and TE}_{01}\ (|l|=1)\\ (|l|-1)\phi+\pi/2 & \mathrm{EH}_{|l|-1,m}\ \text{odd and TM}_{01}\ (|l|=1)\end{cases} \tag{2}$$

In optical fibers, an OAM mode is a linear combination of the degenerate even and odd HE(EH) modes with a relative phase difference of ±π/2; an OAM mode must be circularly polarized. TE_{01} and TM_{01} modes can combine to form an OAM mode, but the OAM mode is usually considered to be "unstable" due to the large effective index separation, Δn_{eff}, between the TE_{01} and TM_{01} modes. For example, the Δn_{eff} between TE_{01} and TM_{01} modes is measured to be ~6.6×10^{-4} in the OAM fiber which has an inverse parabolic graded index profile [18]. The ±1 order OAM modes supported by TE_{01} and TM_{01} modes periodically couple to each other during propagation as will be shown in the following sections. The OAM modes in optical fibers can be expressed as:

$$\begin{cases}\mathrm{OAM}^{\mp}_{\pm|l|,m}=\mathrm{HE}^{even}_{|l|+1,m}\mp i\mathrm{HE}^{odd}_{|l|+1,m}\\ \mathrm{OAM}^{\pm}_{\pm|l|,m}=\mathrm{EH}^{even}_{|l|-1,m}\pm i\mathrm{EH}^{odd}_{|l|-1,m}\end{cases} \tag{3}$$

The superscript "±" over the term "OAM" in (3) represents the handedness of the circular polarization (CP), "+" means right circularly polarized (RCP) and "-" is left circularly polarized (LCP). Here LCP/RCP is defined to be clockwise/counter-clockwise circularly polarized if viewed by the transmitter. For OAM modes formed by HE modes, the handedness of the CP and the OAM are anti-aligned, *i.e.* LCP corresponds to +|l| order OAM and RCP corresponds to -|l| order OAM, while for those formed by EH modes the handedness is aligned. TE_{01}/TM_{01} modes are the same as EH modes. In OAM fibers, since the large effective index separation (>10^{-4}) guarantees negligible cross coupling between HE and EH modes, it is reasonable to assume that the HE and EH supported OAM modes are independent from each other and they can be treated separately as will be done throughout this paper.

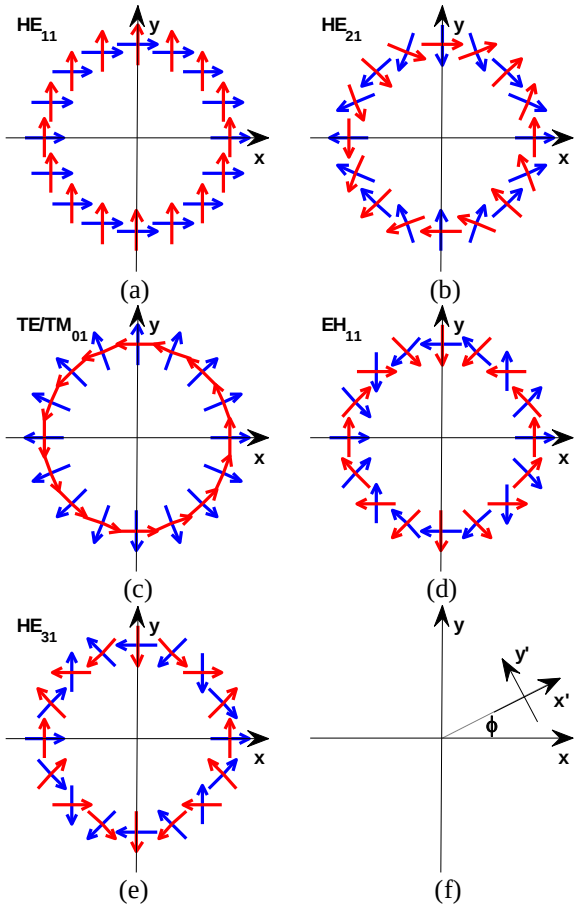

Fig. 1. Schematic diagram of the SOPs of even (blue arrows) and odd (red arrows) vector modes, (a) HE_{11}, (b) HE_{21}, (c) TE_{01} (blue) and TM_{01} (red), (d) EH_{11} and (e) HE_{31}; (f) the Cartesian coordinate system (x, y) and the local coordinate system (x', y').

This article has been accepted for publication in a future issue of this journal, but has not been fully edited. Content may change prior to final publication. Citation information: DOI 10.1109/JLT.2015.2506461, Journal of Lightwave Technology

The SOP of the fundamental modes (HE_{11}) can be described in either Jones or Stokes space. In Jones space, the 2D Jones ket vector $|s\rangle$ is a superposition of the orthogonal x- and y-polarized states, $|s_x\rangle$ and $|s_y\rangle$, respectively [19]:

$$|s\rangle = a|s_x\rangle + b|s_y\rangle \tag{4}$$

where $a=\langle s_x|s\rangle$ and $b=\langle s_y|s\rangle$ are complex quantities, $\langle s|s\rangle=1$. The bra-ket notation is used to distinguish Jones vectors from Stokes vectors. The bra vector, *e.g.* $\langle s|$, indicates the corresponding complex conjugate row vector. The Stokes parameters are:

$$\begin{aligned} s_0^0 &= aa^* + bb^* = |\langle s_x|s\rangle|^2 + |\langle s_y|s\rangle|^2 \\ s_1^0 &= aa^* - bb^* = |\langle s_x|s\rangle|^2 - |\langle s_y|s\rangle|^2 \\ s_2^0 &= ab^* + a^*b = 2\,\mathrm{Re}\left(\langle s_x|s\rangle\langle s|s_y\rangle\right) \\ s_3^0 &= j\left(ab^* - a^*b\right) = 2\,\mathrm{Im}\left(\langle s|s_x\rangle\langle s_y|s\rangle\right) \end{aligned} \tag{5}$$

$\hat{s}^0=\left(s_1^0, s_2^0, s_3^0\right)$ is defined as the Stokes vector for the fundamental modes and * denotes complex conjugation. Fig. 2 plots the corresponding Poincaré sphere. Here the superscript "0" means the topological charge of the OAM carried by the fundamental modes is 0.

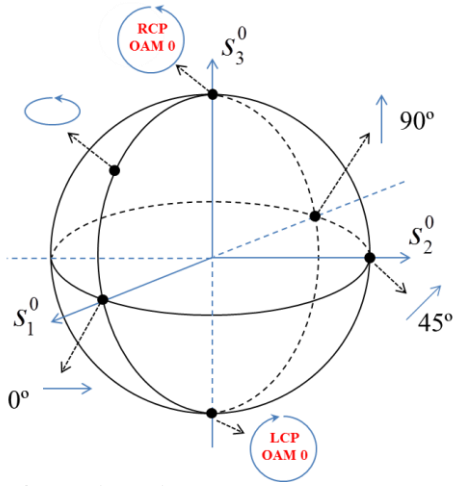

Fig. 2. Poincaré sphere for the fundamental HE_{11} mode.

A higher-order vector mode with a non-zero topological charge $|l|$ is formed from a linear combination of the degenerate even and odd modes, resulting in a complex SOP, denoted by $|s^{\pm|l|}\rangle$ in Jones space. The superscript "±" here denotes the handedness between CP and OAM, "+" means aligned (EH or TE_{01}/TM_{01} modes) and "-" represents anti-aligned (HE modes). Equation (4) then can be extended to higher orders:

$$|s^{\pm|l|}\rangle = a_e^{\pm|l|}|s_e^{\pm|l|}\rangle + b_o^{\pm|l|}|s_o^{\pm|l|}\rangle \tag{6}$$

$|s_e^{\pm|l|}\rangle$ and $|s_o^{\pm|l|}\rangle$ are the SOPs of even (subscript "*e*") and odd (subscript "*o*") modes (or, TE_{01} and TM_{01} modes) respectively. $a_e^{\pm|l|}=\langle s_e^{\pm|l|}|s^{\pm|l|}\rangle$, $b_e^{\pm|l|}=\langle s_o^{\pm|l|}|s^{\pm|l|}\rangle$ and $\langle s^{\pm|l|}|s^{\pm|l|}\rangle=1$. Higher-order Stokes parameters and higher-order Poincaré spheres [20] are then built for each higher-order vector mode in the same way as that of the fundamental HE_{11} mode:

$$\begin{aligned} s_0^{\pm|l|} &= |\langle s_e^{\pm|l|}|s^{\pm|l|}\rangle|^2 + |\langle s_o^{\pm|l|}|s^{\pm|l|}\rangle| \\ s_1^{\pm|l|} &= |\langle s_e^{\pm|l|}|s^{\pm|l|}\rangle|^2 - |\langle s_o^{\pm|l|}|s^{\pm|l|}\rangle|^2 \\ s_2^{\pm|l|} &= 2\,\mathrm{Re}\left(\langle s_e^{\pm|l|}|s^{\pm|l|}\rangle\langle s^{\pm|l|}|s_o^{\pm|l|}\rangle\right) \\ s_3^{\pm|l|} &= 2\,\mathrm{Im}\left(\langle s^{\pm|l|}|s_e^{\pm|l|}\rangle\langle s_o^{\pm|l|}|s^{\pm|l|}\rangle\right) \end{aligned} \tag{7}$$

$\hat{s}^{\pm|l|}=\left(s_1^{\pm|l|}, s_2^{\pm|l|}, s_3^{\pm|l|}\right)$ is the high-order Stokes vector, $\hat{s}^{-|l|}$ is the Stokes vector for the $HE_{|l|+1,m}$ modes and $\hat{s}^{+|l|}$ is for the $EH_{|l|-1,m}$ modes. When $|l|=1$, $\hat{s}^{+1}$ represents the Stokes vector for TE_{01} and TM_{01} modes. When $|l|=0$, Equation (7) converges to (5). On the Poincaré sphere described by (7), the North Pole is always RCP and the south Pole is always LCP. For HE modes, the North Pole has an OAM with topological charge of $-|l|$ and the south Pole carries $+|l|$; while for EH modes, the case is inversed. The intersection between the $s_1^{\pm|l|}$-axis and the sphere represents the even fiber mode; the intersection between the $s_2^{\pm|l|}$-axis and the Sphere means a linear combination of the degenerate even and odd fiber modes with the same phase and intensity. Fig. 3 gives an example of the Poincaré sphere for the HE_{21} mode. Equations (6) and (7) are established based on the orthogonal even and odd vector modes basis so as to make them compatible with that of the fundamental mode ((4) and (5)). It is equivalent to the definition of the higher-order Stokes parameters in [20], which is based on the CP basis.

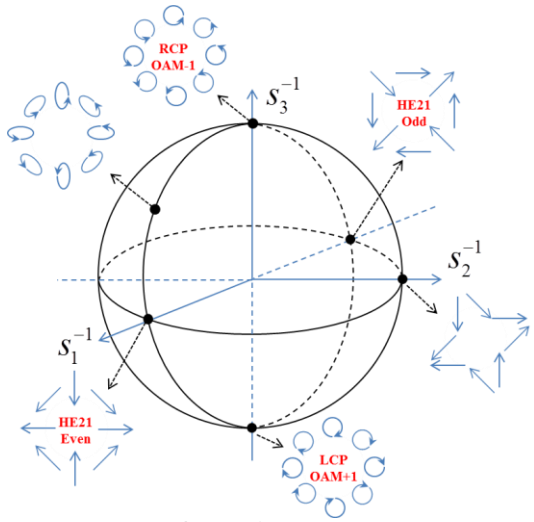

Fig. 3. Higher-order Poincaré sphere for the HE_{21} mode.

III. Modeling of OAM-PMD

PMD is a well-known phenomenon in SMFs. It originates from the birefringence of the fiber and the random variation of its orientation along the fiber length. When the fiber core is not perfectly circular, or when external perturbations such as stress, bending or twisting, are applied on the fiber, the propagation constants of the even and odd fundamental modes separate, giving rise to PMD.

In OAM fibers, the fiber imperfections can also induce modal birefringence to the degenerate even and odd

This article has been accepted for publication in a future issue of this journal, but has not been fully edited. Content may change prior to final publication. Citation information: DOI 10.1109/JLT.2015.2506461, Journal of Lightwave Technology

higher-order HE or EH modes which constitute the OAM modes. Since the stable propagation of an OAM mode requires a fixed ±π/2 phase difference as indicated by (3), the higher-order modal birefringence together with the random variation of the birefringence orientation will result in a random coupling between the *+l* and *–l* order OAM modes along the fiber. Note that this cross coupling only happens between OAM modes supported by the same vector modes, *i.e.*, the CP-OAM handedness should be either aligned or anti-aligned. This is because the HE and EH modes are assumed to be isolated in OAM fibers as discussed in Section II. The OAM-PMD here is a special case of the MD in [15], where the 3*N*-dimentional Stokes space (MD) is simplified into *N* independent 3-dimentional Stokes spaces (OAM-PMD).

A. Fixed-Birefringence Model

Similar to SMFs, the OAM-PMD in OAM-fibers can be modeled in two ways. The fiber is considered to be a concatenation of a large number of birefringence fiber sections [21]–[23]. In the first model, the birefringence magnitude is a constant for all the sections, but the orientation angle ϕ of the fiber sections is random (Fig. 4). In the second model both the magnitude and angle are random. Since the two models give similar statistical results, we use the first one in this paper for simplicity.

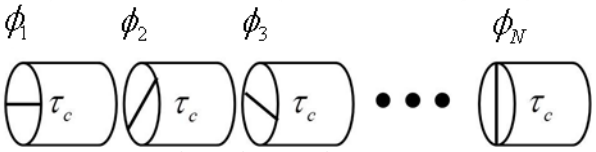

Fig. 4. Schematic diagram for the fixed-birefringence model, where τ_C is the differential group delay of one single fiber section.

The evolution of the Stokes vector with respect to length and optical frequency corresponding to a specific vector mode obeys the precession rules:

$$\frac{d\hat{s}^{\pm|l|}}{dz} = \vec{\beta}^{\pm|l|} \times \hat{s}^{\pm|l|} \tag{8}$$

$$\frac{d\hat{s}^{\pm|l|}}{d\omega} = \vec{\tau}^{\pm|l|} \times \hat{s}^{\pm|l|} \tag{9}$$

where $\vec{\tau}^{\pm|l|}$ is the cumulative OAM-PMD vector up to position *z* and $\vec{\beta}^{\pm|l|} = \left(\beta_1^{\pm|l|}, \beta_2^{\pm|l|}, \beta_3^{\pm|l|}\right)$ is the local birefringence vector at position *z*, which has a magnitude of $\left|\vec{\beta}^{\pm|l|}\right|$. Here we assume that there is no circular birefringence, *i.e.* $\beta_3^{\pm|l|} = 0$, and $\vec{\beta}^{\pm|l|}$ is always in the plane defined by the equator of the Poincaré sphere. The orientation of $\vec{\beta}^{\pm|l|}$ can then be defined by the angle between $\vec{\beta}^{\pm|l|}$ and the $s_1^{\pm|l|}$-axis in the Stokes space, θ_C. $\vec{\beta}^{\pm|l|}$ is different for different vector modes in terms of both the magnitude and the orientation. $\left|\vec{\beta}^{\pm|l|}\right| = 2\pi / L_B^{\pm|l|}$, $L_B^{\pm|l|}$ is the local modal beat length. θ_C is related to the modal birefringence correlation length $L_C^{\pm|l|}$ which will be discussed in detail below.

B. Birefringence Correlation Length

In the fixed-birefringence model, θ_C is assumed to be a Brownian motion [24]:

$$\begin{cases} \dfrac{d\theta_C}{dz} = g_\theta(z) \\ \left\langle g_\theta(z) \right\rangle = 0 \\ \left\langle g_\theta(z)\, g_\theta(z') \right\rangle = \sigma_\theta^2 \delta(z - z') \end{cases} \tag{10}$$

$g_\theta(z)$ is a white-noise stochastic process. The autocorrelation of θ_C is calculated to be $\exp(-\sigma_\theta^2 z/2)$. The birefringence correlation length L_C is defined as the length at which the autocorrelation of θ_C falls to e^{-1}, *i.e.* $L_C^{\pm|l|} = 2/\sigma_\theta^2$. Considering two cascaded birefringent fiber sections, the first section is set to be the reference; in Stokes space its birefringence vector superimposes the $s_1^{\pm|l|}$-axis. In the local Cartesian coordinate system (x', y'), the orientations of the modal electrical fields of the first section, θ_1', is described by (2). Assuming the second fiber section is rotated clockwise (viewed by the transmitter) by an angle of $\Delta\phi$ with respect to the first section, the orientation of its modal electrical fields becomes $\theta_2' = \theta_1'(\phi + \Delta\phi)$ and θ_C can be calculated as:

$$\begin{aligned} \theta_C &= 2\left(\theta_2' - \theta_1'\right) = 2\left(\theta_1'(\phi + \Delta\phi) - \theta_1'(\phi)\right) \\ &= \begin{cases} -2\left(|l|+1\right)\Delta\phi & \mathrm{HE}_{|l|+1,m} \\ 2\left(|l|-1\right)\Delta\phi & \mathrm{EH}_{|l|-1,m},\ \mathrm{TE}_{01}/\mathrm{TM}_{01}\ (|l|=1) \end{cases} \end{aligned} \tag{11}$$

For the fundamental mode, $|l|=1$, $\theta_C = -2\Delta\phi$. For the other modes, there is a scaling factor $|l|\pm 1$. According to (10), this scaling factor would also be transferred to $g_\theta(z)$. As a result, the modal birefringence correlation length is dependent on the topological charge *l*:

$$L_C^{\pm|l|} = \frac{2}{\left(|l| \pm 1\right)^2 \left(\sigma_\theta^0\right)^2} = \frac{L_C^0}{\left(|l| \pm 1\right)^2} \quad \begin{pmatrix} \text{+ sign for } \mathrm{HE}_{|l|+1} \\ \text{- sign for } \mathrm{EH}_{|l|-1} \text{ and } \mathrm{TE}_{01}/\mathrm{TM}_{01}(|l|=1) \end{pmatrix} \tag{12}$$

where L_C^0 is the birefringence correlation length of the fundamental HE_{11} mode. The superscript "±" over the term L_C accounts for the CP-OAM handedness, the same as that for $\hat{s}^{\pm|l|}$. A special case exists for the TE_{01}/TM_{01} mode. As shown by Fig. 1 (c) the polarization states of TE_{01} and TM_{01} modes are independent of the azimuthal angle. The random orientation of the fiber sections shown in Fig. 4 will not induce any mode coupling between the TE_{01} and TM_{01} modes. Therefore the TE_{01} and TM_{01} modes of an OAM fiber will have infinite correlation length as indicated by (12) (the denominator becomes zero). The *l* and *–l* order OAM modes supported by TE_{01}/TM_{01} modes periodically couple to each other. The scaling effect of the modal birefringence correlation length can be explained physically as follows: the "strength" of the white-noise g_θ, σ_θ^2, generally increases with the increase of the topological charge *l* under the same random variation of the fiber section's orientation; the stronger the noise the shorter the fiber length necessary to reach a nearly uniform angular distribution of θ_C between $-\pi/2$ and $\pi/2$.

This article has been accepted for publication in a future issue of this journal, but has not been fully edited. Content may change prior to final publication. Citation information: DOI 10.1109/JLT.2015.2506461, Journal of Lightwave Technology

C. Mean value of OAM-PMD

To find the mean value of OAM-PMD, we first take the frequency derivative of (8) and the position derivative of (9). Due to the continuity of the function $\hat{s}(z,\omega)$, the two derivatives should be equal. Using the identity $\left(\vec{\beta}^{\pm|l|}\times\vec{\tau}^{\pm|l|}\right)\times\hat{s}^{\pm|l|}=\vec{\beta}^{\pm|l|}\times\left(\vec{\tau}^{\pm|l|}\times\hat{s}^{\pm|l|}\right)-\vec{\tau}^{\pm|l|}\times\left(\vec{\beta}^{\pm|l|}\times\hat{s}^{\pm|l|}\right)$, the differential equation determining the motion of the OAM-PMD vector $\vec{\tau}$ is derived as:

$$\frac{\partial\vec{\tau}^{\pm|l|}}{\partial z}=\vec{\beta}_{\omega}^{\pm|l|}+\vec{\beta}^{\pm|l|}\times\hat{s}^{\pm|l|} \tag{13}$$

The solution of (13) is the mean value of OAM-PMD, $<\tau^{\pm|l|}>$, which is a function of the modal beat length $L_B^{\pm|l|}$ and the modal birefringence correlation length $L_C^{\pm|l|}$:

$$\left\langle\tau^{\pm|l|}\right\rangle^2=\frac{16}{3\pi}\left(\frac{\lambda L_C^{\pm|l|}}{cL_B^{\pm|l|}}\right)^2\left(\exp\left(-z/L_C^{\pm|l|}\right)+z/L_C^{\pm|l|}-1\right) \tag{14}$$

The detailed derivation of (14) based on the fixed-birefringence model can be found on Chapter 9 (pp.399) in [24]. From (14) we can see that $<\tau^{\pm|l|}>$ is approximately proportional to $L_C^{\pm|l|}$ and is inversely proportional to $L_B^{\pm|l|}$. Considering the scaling effect of $L_C^{\pm|l|}$, higher order OAM modes should show smaller OAM-PMD. Furthermore recent research has found that the external perturbations such as bending affect mostly lower order OAM modes [11]. In other words, $L_B^{\pm|l|}$ is intrinsically smaller for higher order OAM modes. Therefore, higher order OAMs modes should be more stable in OAM fibers.

IV. Measurement and Characterization of OAM Fibers

The PMD is characterized by the PMD vector $\vec{\tau}$ which varies randomly with respect to the optical frequency. The mean value of PMD, $<\tau^{\pm|l|}>$, is the PMD feature that is of the most interest to measure, as it is a very useful predictor of performance that does not change from day to day or from fiber to fiber. For SMFs, the fixed-analyzer technique is the simplest and widely-used technique for measuring the mean value of PMD [25]. As discussed in Section III, the OAM-PMD in OAM fibers obeys the same precession rules ((8) and (9)) as those for the fundamental modes in SMFs, thus the fixed-analyzer technique can in principle be applied for the measurement of $<\tau^{\pm|l|}>$. In this section, we characterize the OAM-PMD of two different types of OAM-fibers, namely a graded index fiber with an inverse parabolic profile and a ring-core fiber with a step index profile. We perform the measurement for different orders of OAM modes. To explain the differences observed in OAM-PMD, we further investigate the birefringence of OAM fibers, first through numerical simulations and then through measurement of the local birefringence using optical backscattering reflectometry.

A. Measurement principle and experimental setup

As shown in Fig. 5, a C-band ASE (amplified spontaneous emission) light from an EDFA was used as the broadband laser source. The light was polarized by passing through a polarizer and was converted to an l order OAM beam after reflection by an appropriately programmed spatial light modulator (SLM1). Before being coupled into the OAM fiber, the light is converted to CP via a quarter-wave plate (Q1). By programing SLM1 and rotating Q1, an OAM mode with a topological charge l and a specific CP-OAM handedness can be selectively excited in the OAM fiber under test. After propagating through the OAM fiber, the OAM mode is subjected to OAM-PMD, *i.e.* the $\pm l$ order OAM modes with the same CP-OAM handedness (supported by the same vector modes) would randomly couple to each other resulting in a mixture of $\pm l$ order OAM modes and a complex SOP at the output of the fiber. As the optical frequency changes, the Stokes vector of the output light $\hat{s}^{\pm|l|}$ randomly moves on the corresponding higher-order Poincaré sphere.

The receiver was set to only detect either RCP or LCP OAM mode, with the CP-OAM handedness kept the same as that of the input. The receiver in the experimental setup can be considered as an "OAM-polarizer" whose Stokes vector $\hat{p}^{\pm|l|}$ aligns with the $s_3^{\pm|l|}$-axis pointing to either the north (RCP) or south (LCP) pole. The spectrum recorded by the optical spectrum analyzer (OSA) is actually the projection of the output Stokes vector on $\hat{p}^{\pm|l|}$:

$$T^{\pm|l|}(\omega)=\frac{1}{2}\left[1+\hat{s}^{\pm|l|}(\omega)\bullet\hat{p}^{\pm|l|}\right] \tag{15}$$

Poole *et al.* proved that the mean value of the differential group delay (equivalent to $<\tau^{\pm|l|}>$ in this paper) is proportional to the density of extrema in the spectrum $T^{\pm|l|}(\omega)$ [26]:

$$\left\langle\tau^{\pm|l|}\right\rangle=0.805\pi\frac{\left\langle N_e^{\pm|l|}\right\rangle}{\Delta\omega} \tag{16}$$

$<N_e^{\pm|l|}>$ is the mean value of the number of extrema and $\Delta\omega$ is the optical angular frequency range over which the measurement is taken. The coefficient 0.805 in (16) is reported by Williams [26] which is a correction to the original factor of 0.824 reported in [25]. In the experiment, we use the measured number of extrema, $N_e^{\pm|l|}$, as an approximation to $<N_e^{\pm|l|}>$. Because of the finite measurement frequency range $\Delta\omega$, there is an uncertainty of the measurement results. As derived in [25], the uncertainty η

$$\eta\approx\frac{0.52}{N_e} \tag{17}$$

is inversely proportional to the number of extrema.

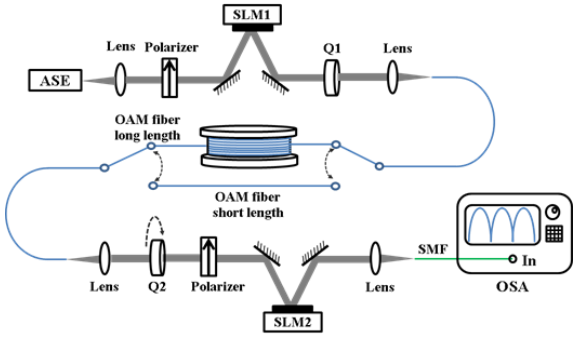

Fig. 5. Experimental setup for measuring of $<\tau^{\pm|l|}>$. SLM: spatial light modulator, Q: quarter-wave plate, ASE: amplified spontaneous emission source, OSA: optical spectrum analyzer.

B. OAM fibers to be characterized

We used the technique proposed above (as shown in Fig. 6)

This article has been accepted for publication in a future issue of this journal, but has not been fully edited. Content may change prior to final publication. Citation information: DOI 10.1109/JLT.2015.2506461, Journal of Lightwave Technology

to characterize two types of OAM fibers designed and fabricated in our lab. The first OAM fiber has an inverse-parabolic graded index profile, referred to as "IPGIF" [9]. Its refractive index profile is expressed as:

$$n(r)=\begin{cases} n_1\sqrt{1-2N\Delta\left(r^2/a^2\right)}, & 0\le r\le a \\ n_2, & r>a \end{cases} \quad (18)$$

$N=(n_1-n_a)/(n_1-n_2)=-4$, which is the curvature parameter; $n_a=1.494$ is the maximal refractive index of the ring area; $n_1=1.454$ is the refractive index at the fiber center; $n_2=1.444$ is the refractive index of the cladding; $\Delta=(n_1^2-n_2^2)/2n_1^2$ is the relative permittivity contrast; a is the ring radius which equals 3 μm. IPGIF supports up to the second order OAM modes (HE_{11}, TE_{01}, HE_{21}, TM_{01}, EH_{11} and HE_{31}). However the second order OAM modes supported by EH_{11} and HE_{31} modes are close to cutoff [9]. Thus the zero and first order OAM mode supported by HE_{11} and HE_{21} modes respectively are of the most interest for data transmission.

The other OAM fiber to be measured has a ring-shaped step-index profile, referred to as "RCF" [27]. It has an inner-ring radius of 0.97 μm and an outer-ring radius of 2.44 μm. The refractive index of the ring is 1.474 and that of the cladding is the same as IPGIF (pure silica). RCF supports up to the first order OAM modes (HE_{11}, TE_{01}, HE_{21} and TM_{01}).

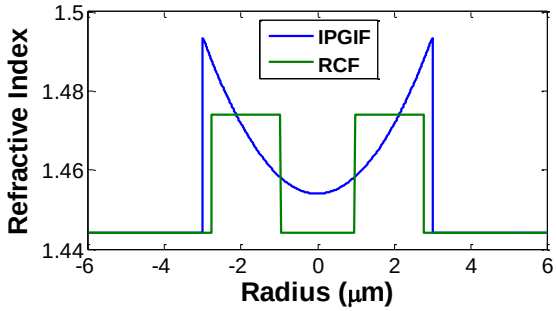

Fig. 6. Refractive index profiles for the inverse-parabolic graded index fiber (IPGIF) and the ring-core step-index fiber (RCF).

C. *Measurement of mean value of OAM-PMD*

Before measuring the OAM-PMD of OAM fibers with long lengths, we measured the differential group delay between the TE_{01} and TM_{01} modes over short length of fibers (a few meters). As mentioned in Section III, OAM fibers perform like a conventional PMF for the TE_{01} and TM_{01} modes. To excite the TE_{01} and TM_{01} modes simultaneously, +/-1 order RCP/LCP OAM mode were generated and coupled into the OAM fiber. At the receiver end, SLM2 and Q2 were set to convert the +/-1 order RCP/LCP OAM mode back into a linearly polarized fundamental Gaussian beam to be received by a SMF pigtail and recorded by the OSA. Because the two vector modes have a large index separation, the recorded transmission spectra show pure cosine shapes. The IPGIF under test is 4.6 m, while the RCF is 5.3 m. The measured spectra are shown in Fig. 7 and Fig. 8 respectively. The time delay TE_{01} and TM_{01} modes can be read from the period of the spectra. For IPGIF the delay is 1.4 ps/m and for RCF it is 2.52 ps/m.

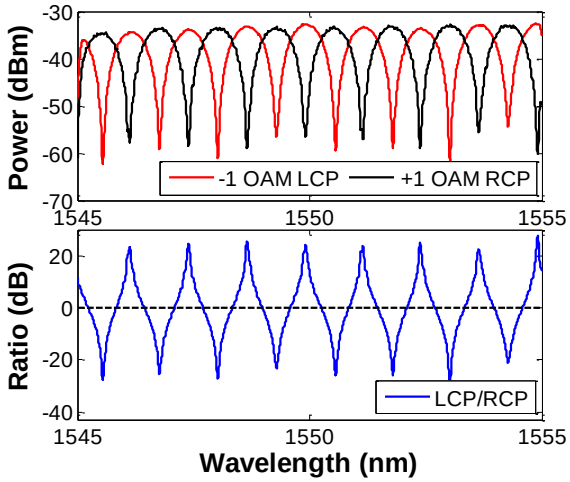

Fig. 7. Measured transmission spectra for the TE_{01} and TM_{01} modes over IPGIF with a length of 4.6 m.

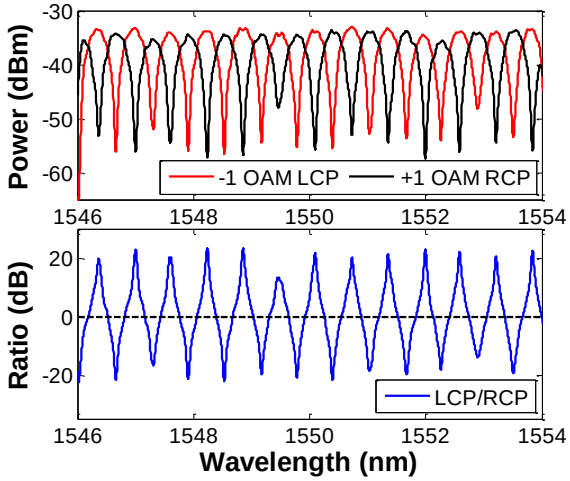

Fig. 8. Measured transmission spectra for the TE_{01} and TM_{01} modes over RCF with a length of 5.3 m.

To verify the measurement results of TE_{01} and TM_{01} modes using the fixed-analyzer technique, a time of flight (ToF) measurement was taken for long fibers (1.09 km for IPGIF and 1.59 km for RCF). A pulsed laser source with a pulse width ~ 100ps and a repetition rate of ~19.5 MHz was generated by externally modulating a continuous-wave (CW) laser source (1550 nm) in a Mach-Zehnder optical intensity modular. The laser pulse train was coupled into the OAM fiber through free-space optics. The alignment was intentionally offset so as to excite all the vector modes in the fiber. At the receiver end, a high-speed photodetector together with an electrical sampling scope were used to detect the output optical pulses.

The ToF measurement of IPGIF clearly shows four peaks (Fig. 9), corresponding to HE_{11}, TE_{01}, HE_{21} and TM_{01} modes. The peaks for EH_{11} and HE_{31} modes are too weak to be observed. The ToF measurement of RCF also shows four peaks (Fig. 10). The measured time delays between the TE_{01} and TM_{01} modes after propagating through the OAM fibers are 1.57 ns for 1.09 km IPGIF (1.44 ps/m) and 4.12 ns for 1.59 km RCF (2.59 ps/m), matching with those obtained by the fixed-analyzer technique. This indicates that, in the setup shown in Fig. 5, the free space optics in both the transmitter and the receiver were

This article has been accepted for publication in a future issue of this journal, but has not been fully edited. Content may change prior to final publication. Citation information: DOI 10.1109/JLT.2015.2506461, Journal of Lightwave Technology

well aligned so that TE_{01} and TM_{01} modes were excited and detected with relatively high mode purity.

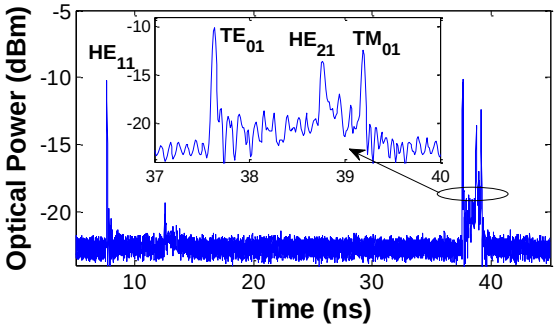

Fig. 9. Time of flight measurement results for the TE_{01} and TM_{01} modes over IPGIF with a length of 1.09 km.

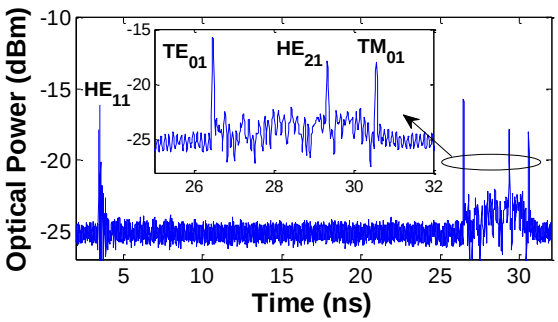

Fig. 10. Time of flight measurement results for the TE_{01} and TM_{01} modes over RCF with a length of 1.59 km.

Afterwards the SLMs and the quarter-wave plates were set to generate and detect other OAM modes supported by HE/EH modes over the short OAM fiber. The free space optics was finely adjusted until the curve shown on the screen of the OSA became as smooth as possible. This calibration process guarantees an optimized condition (high mode purity) for the excitation and detection of a specific OAM mode. Then the short fiber was cut in the center and the long length of fiber was inserted by fusion splicing. By doing so the already well-aligned free space optics was kept untouched. Fig. 11 shows the measured transmission spectra for OAM modes with different orders and different directions of CP in 1.09 km IPGIF. The red and black curves are the spectra measured when the receiver was set to detect *l* order OAM modes with LCP and RCP respectively. The impact of the spectral shape of the ASE source has been removed from the raw data. The blue curve is the ratio between the LCP and RCP spectra. Fig. 12 shows the results for 1.59 km RCF.

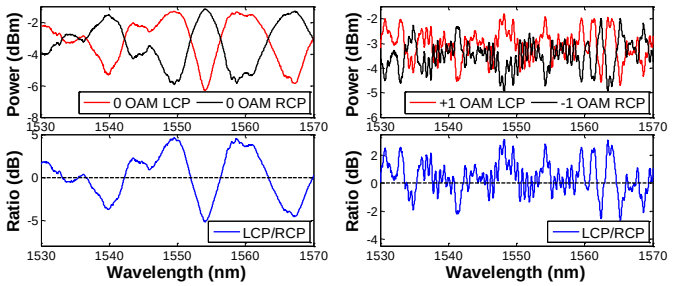

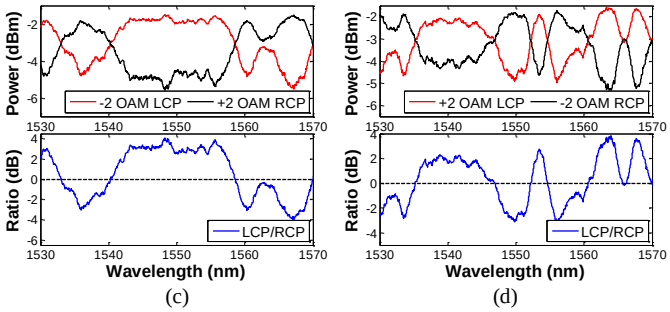

Fig. 11. Measured transmission spectra for OAM modes supported by (a) HE_{11}, (b) HE_{21}, (c) EH_{11} and (d) HE_{31} modes over IPGIF with a length of 1.09 km.

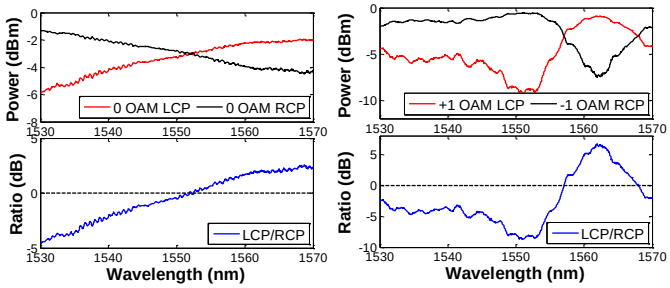

Fig. 12. Measured transmission spectra for OAM modes supported by (a) HE_{11} and (b) HE_{21} modes over RCF with a length of 1.59 km.

TABLE 1
Summary of the measurement results

	IPGIF 1.09 km			RCF 1.59 km		
Modes	N_e	$<\tau^{\pm\|l\|}>$	η	N_e	$<\tau^{\pm\|l\|}>$	η
HE_{11}	10	0.80 ps	5.2%	1	0.08*	52%*
HE_{21}	104	8.34 ps	0.5%	3	0.24*	17%*
EH_{11}	6	0.48 ps	8.67%			
HE_{31}	11	0.88 ps	4.73%			
TE_{01} /TM_{01}	--	1.4 ps/m			2.52 ps/m	

* For RCF, the values calculated from (16) and (17) provide only a rough estimation because the number of extrema over the measurement frequency range is too small to give accurate results.

The measured values of $<\tau^{\pm|l|}>$ for IPGIF and RCF are summarized in TABLE 1. For the 1.59 km long RCF, the transmission spectra for the 0 order (HE_{11}) and 1 order (HE_{21}) OAM modes only show 1 and 3 extrema over the 40 nm wavelength range, which is too small to give an accurate estimation of the OAM-PMD. In comparison, IPGIF shows much larger OAM-PMDs. Fig. 13 shows the simulated modal birefringence of IPGIF and RCF as a function of core ellipticity using a finite element solver (COMSOL). The ellipticity is defined as the ratio of the major to the minor axes. The ellipticity-induced δn_{eff} are similar for IPGIF and RCF. Since $<\tau^{\pm|l|}>$ is proportional to δn_{eff} ((14)), the large discrepancy of the measured $<\tau^{\pm|l|}>$ between IPGIF and RCF does not come from the fiber designs. It should be noted that, although the elliptical core induces modal birefringence to the originally degenerate even and odd modes, the Δn_{eff} between HE, EH, TE_{01} and TM_{01} modes only change slightly and are always $>10^{-4}$ throughout the parameter sweeping (the ellipticity sweeps from 1 to 1.04).

This article has been accepted for publication in a future issue of this journal, but has not been fully edited. Content may change prior to final publication. Citation information: DOI 10.1109/JLT.2015.2506461, Journal of Lightwave Technology

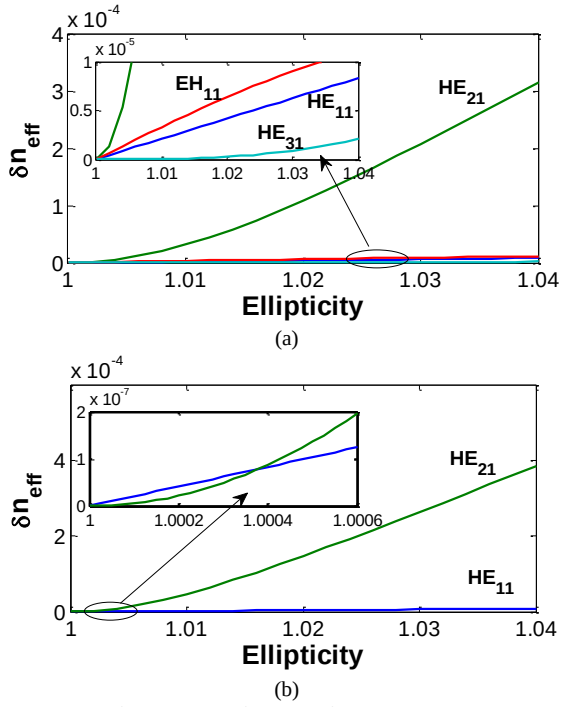

Fig. 13. Modal birefringence as a function of the core ellipticity (simulations). (a) IPGIF, which supports up to the ±2 order OAM modes, (b) RCF which supports up to ±1 order OAM modes.

D. *Measurement of beat lengths*

To further investigate the discrepancy between IPGIF and RCF, we next measured the local beat lengths of the fundamental HE_{11} modes (L_B^0) using the optical backscatter reflectometer (OBR 4400) from Luna Technologies [28]. The experimental setup is plotted in Fig. 14. The output SMF pigtail of the OBR was center-to-center fusion spliced with the OAM fiber so as to excite mostly the HE_{11} modes. The OAM fiber was then coiled for a few turns along a rod with a diameter of ~2 cm to further remove the higher order modes. The Rayleigh scattering passed through a built-in polarizer and was mixed with the local tunable laser source (TLS) and detected by an optical coherent receiver. The other end of the OAM fiber was immersed in the index matching oil (IMO) for removing any facet reflection. The amplitude of the time-domain data of the OBR is equivalent to a traditional optical time domain reflectometry (OTDR) measurement. The measured Rayleigh backscattering intensity contains periods equal to the beat length L_B^0 and to $L_B^0/2$ [28]. By applying an FFT to the backscattering intensity, the local beat length can be obtained. For IPGIF, the FFT was performed at each position with a step of 1 m and a FFT window of 10 m, while for RCF the window was set to 300 m wide. Fig. 15 (a) gives an example of the FFT spectrum of IPGIF at the position of 25 m. It shows clearly two peaks corresponding to L_B^0 and $L_B^0/2$ respectively. The FFT spectrum of RCF is a bit noisy but the peak corresponding to $L_B^0/2$ is still significant. Fig. 15 (b) shows the FFT spectrum of RCF at the position of 100m. The measured local beat lengths along the fiber were averaged to obtain the mean-value of beat lengths, $\langle L_B^0 \rangle$, For IPFIG, $\langle L_B^0 \rangle$=0.34 m ($\langle \delta n_{eff}^0 \rangle$=4.6×10^{-6}). $\langle L_B^0 \rangle$ of RCF is 16.7 m ($\langle \delta n_{eff}^0 \rangle$=9.3×10^{-8}), which is much longer than that of IPGIF. This result explains the large discrepancy between the measured $\langle \tau^{\pm|l|} \rangle$ of IPGIF and RCF. The very short $\langle L_B^0 \rangle$ in IPGIF may come from the fiber fabrication process and needs further investigations.

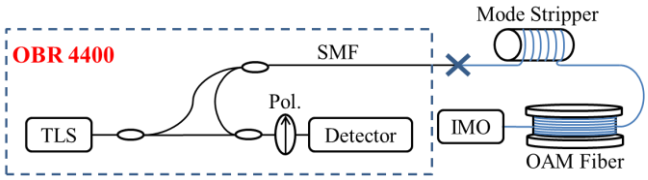

Fig. 14. Experimental setup for measuring the local beat lengths of the fundamental mode (HE_{11}) using optical frequency-domain reflectometry. TLS: tunable laser source, Pol.: polarizer, IMO: index matching oil.

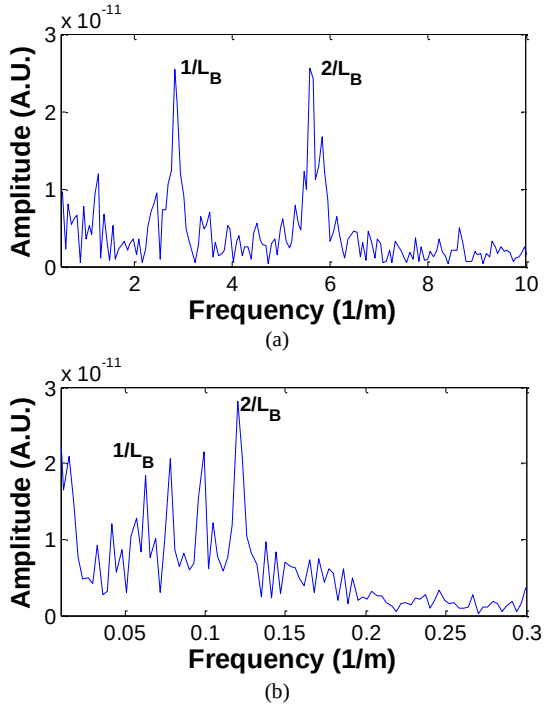

Fig. 15. FFT spectrum of the Rayleigh scattering of (a) IPGIF at the position of 25 m with a FFT window of 10 m; (b) RCF at the position of 100 m with a FFT window of 300 m.

V. Discussion

As presented in section III, the value $\langle \tau^{\pm|l|} \rangle$ varies with respect to the topological charge l of OAM modes. Furthermore, it is determined by both the modal beat length $L_B^{\pm|l|}$ ($L_B^{\pm|l|} = \lambda/\delta n_{eff}^{\pm|l|}$, λ is the wavelength and $\delta n_{eff}^{\pm|l|}$ is the modal birefringence) and the modal birefringence correlation length ((14)). Based on the measured $\langle L_B^0 \rangle$ and $\langle \tau^0 \rangle$ of the fundamental mode (0 order OAM mode), the birefringence correlation length, L_C^0, can be calculated using (14). Assuming that the modal birefringence originates only from the core ellipticity, we can then find out the beat lengths of the higher-order OAM modes, $L_B^{\pm|l|}$, using the simulation results shown in Fig. 13, and also find out the higher-order birefringence correlation, $L_C^{\pm|l|}$, using the scaling rule as shown by (12). Finally, using (14) again, $\langle \tau^{\pm|l|} \rangle$ for all the higher-order OAM modes can be calculated. TABLE 2 lists the measured (bold) and calculated (italic) $\langle \tau^{\pm|l|} \rangle$ of IPGIF. For the ±1 order OAM modes supported by the HE_{21} modes, the measurement ($\langle \tau^{-1} \rangle$=8.34 ps) and the theory ($\langle \tau^{-1} \rangle$ = 11.05 ps) match well.

This article has been accepted for publication in a future issue of this journal, but has not been fully edited. Content may change prior to final publication. Citation information: DOI 10.1109/JLT.2015.2506461, Journal of Lightwave Technology

Regarding the ±2 order OAM modes supported by the EH_{11} modes, the theoretical calculation ($<\tau^{+2}>$ =1.2 ps) is about 2 times the measurement ($<\tau^{+2}>$=0.48 ps) but they are still on the same order of magnitude. Theoretically, $<\tau^{-2}>$, which corresponds to the ±2 order OAM modes supported by the HE_{31} modes, should be much smaller than $<\tau^{0}>$, $<\tau^{-1}>$ and $<\tau^{+2}>$ because 1) the numerical simulation shows the modal birefringence of HE_{31} modes the smallest (Fig. 13 (a)); 2) a scaling factor of 1/9 shortens its birefringence correlation length L_C^{-2} by 9 times compared to L_C^{0}, consequently reducing $<\tau^{-2}>$ further. However, the measured value of $<\tau^{-2}>$ is much larger (0.88 ps). Actually the 2nd order OAM mode was not optimized when we were designing IPGIF. The EH_{11} and HE_{31} modes are close to cutoff [9] and are more lossy than other modes in IPGIF. Moreover, the 2nd mode group lies in the strongly normal chromatic dispersion region (<-100 ps/nm/km). After propagating through the fiber it is highly possible that there was mode coupling between the EH_{11} and HE_{31} modes considering that the length of the OAM fiber is relatively long ~1.09 km. For the sake of comparison, RCF was also investigated in the same way as IPGIF (see TABLE 3). The discrepancy between the measured (0.24 ps) and calculated (0.05 ps) values of $<\tau^{-1}>$ (OAM-PMD of the HE_{21} modes) is acceptable considering that the measured values of OAM-PMD of RCF have restricted accuracy due to the limited measurement wavelength range (Fig. 12).

The key advantage of using OAM modes is that it is able to simplify the multiple-input multiple-output (MIMO) processing in the receiver because the OAM channels supported by different fiber vector modes are non-degenerate and independent of one another. However, the effect of OAM-PMD would induce random coupling and time delay between the ±l order OAM modes supported by the same vector modes. In the experiment of OAM-division-multiplexing demonstrated in [6], this mode coupling was small enough to be compensated by fiber-based polarization controllers, thus no MIMO was implemented. But as the fiber becomes longer or if the OAM-PMD is large, polarization controllers will no longer be sufficient for compensation and N 2×2 MIMO will have to be used for 2N OAM channels. In addition, the complexity of MIMO processing increases as the OAM-PMD increases, which is similar to the case of polarization-division multiplexing in SMFs. Therefore, small values of OAM-PMD are highly desirable in the design and fabrication of OAM fibers.

Multiplexing signals on higher order OAM modes may be a simple and intuitive solution for reducing OAM-PMD because, as discussed in Section III.C, when the OAM order increases, the birefringence correlation length L_C shrinks dramatically while the beat length L_B increases. For OAM modes located in the region of $L_C << L_B$, the direction of the birefringence vector changes rapidly resulting in a very small OAM-PMD. It is similar to the effect exploited in the manufacture of ultra-low PMD SMFs: the fiber geometry and stresses are designed to lengthen the beat length and fiber spinning is intentionally induced during the fabrication process to shorten the birefringence correlation length [29].

TABLE 2
Comparison of the measurement and theoretical calculations for 1.09 km IPGIF

	IPGIF 1.09 km				
Modes	L_B **/m**	$<\delta n_{eff}>$	L_C **/m**	$<\tau^{\pm\|l\|}>$ **/ps**	
				Measured	**Calculated**
HE_{11}	**0.34**	**4.6×10^{-6}**	*1.47*	**0.80**	--
HE_{21}	*0.012*	*1.27×10^{-4}*	*0.37*	**8.34**	*11.05*
EH_{11}	*0.22*	*6.94×10^{-6}*	*1.47*	**0.48**	*1.2*
HE_{31}	*4.38*	*3.54×10^{-7}*	*0.16*	**0.88**	*0.02*

* The bold are measurement results; the italic are the calculated values.

TABLE 3
Comparison of the measurement and theoretical calculations for 1.59 km RCF

	RCF 1.59 km				
Modes	L_B **/m**	$<\delta n_{eff}>$	L_C **/m**	$<\tau^{\pm\|l\|}>$ **/ps**	
				Measured	**Calculated**
HE_{11}	**16.67**	**9.3×10^{-8}**	*25.5*	**0.08**	--
HE_{21}	*13.7*	*1.13×10^{-7}*	*6.38*	**0.24**	*0.05*

* The bold are measurement results; the italic are the calculated values.

VI. Conclusion

In this paper, we generalize the concept of PMD in SMFs to OAM modes in OAM fibers. The OAM-PMD results from a random cross-coupling and frequency-dependent time delay between the $+l$ and $-l$ order OAM modes with the same CP-OAM handedness. It can be described in a number of independent 3D higher-order Stokes spaces. Moreover, we extend the fixed-analyzer technique, which has been widely used in SMFs, to measure the mean-value of OAM-PMD. Two different types of OAM fibers are characterized, IPGIF and RCF. The measurement is compared with the theoretical calculation showing generally good agreement.

The OAM-PMD is a critical factor that indicates the stability of OAM modes in optical fibers, in addition to the effective index separation between HE and EH modes, which has already been accepted as a design target of OAM fibers. The OAM-PMD must be taken into account when developing novel OAM fibers. The measurement of OAM-PMD should provide both a valuable feedback for the optimization of the fiber design and fabrication, and a useful tool for predicting the performance of an OAM-division multiplexing system.

Acknowledgment

This work was supported by the Canada Research Chair in Advanced photonic technologies for communications (APTEC), by the Canada Excellence Research Chair in Enabling photonic innovations for information and communications (CERCP) and by the Natural sciences and engineering research council of Canada (NSERC). It is part of the European Union's Horizon 2020 research and innovation project ROAM, under grant agreement No 645361.

References

[1] L. Allen, M. W. Beijersbergen, R. J. C. Spreeuw, and J. P. Woerdman, "Orbital angular momentum of light and the transformation of Laguerre-Gaussian laser modes," *Phys. Rev. A*, vol. 45, no. 11, pp. 8185–8189, Jun. 1992.

[2] A. E. Willner, J. Wang, and H. Huang, "A Different Angle on Light Communications," *Science (80-.).*, vol. 337, no. 6095, pp. 655–656, Aug. 2012.

[3] G. Gibson, J. Courtial, M. J. Padgett, M. Vasnetsov, V. Pas'ko, S. M. Barnett, and S. Franke-Arnold, "Free-space information transfer using

light beams carrying orbital angular momentum," *Opt. Express*, vol. 12, no. 22, p. 5448, Nov. 2004.
[4] J. Wang, J.-Y. Yang, I. M. Fazal, N. Ahmed, Y. Yan, H. Huang, Y. Ren, Y. Yue, S. Dolinar, M. Tur, and A. E. Willner, "Terabit free-space data transmission employing orbital angular momentum multiplexing," *Nat. Photonics*, vol. 6, no. 7, pp. 488–496, Jun. 2012.
[5] H. Huang, G. Xie, Y. Yan, N. Ahmed, Y. Ren, Y. Yue, D. Rogawski, M. J. Willner, B. I. Erkmen, K. M. Birnbaum, S. J. Dolinar, M. P. J. Lavery, M. J. Padgett, M. Tur, and A. E. Willner, "100 Tbit/s free-space data link enabled by three-dimensional multiplexing of orbital angular momentum, polarization, and wavelength.," *Opt. Lett.*, vol. 39, no. 2, pp. 197–200, Jan. 2014.
[6] N. Bozinovic, Y. Yue, Y. Ren, M. Tur, P. Kristensen, H. Huang, A. E. Willner, and S. Ramachandran, "Terabit-scale orbital angular momentum mode division multiplexing in fibers.," *Science*, vol. 340, no. 6140, pp. 1545–8, Jun. 2013.
[7] S. Ramachandran and P. Kristensen, "Optical vortices in fiber," *Nanophotonics*, vol. 2, no. 5–6, pp. 455–474, Jan. 2013.
[8] N. Bozinovic, S. Golowich, P. Kristensen, and S. Ramachandran, "Control of orbital angular momentum of light with optical fibers.," *Opt. Lett.*, vol. 37, no. 13, pp. 2451–3, Jul. 2012.
[9] B. Ung, P. Vaity, L. Wang, Y. Messaddeq, L. A. Rusch, and S. LaRochelle, "Few-mode fiber with inverse-parabolic graded-index profile for transmission of OAM-carrying modes.," *Opt. Express*, vol. 22, no. 15, pp. 18044–18055, Jul. 2014.
[10] C. Brunet, B. Ung, L. Wang, Y. Messaddeq, S. LaRochelle, and L. A. Rusch, "Design of a family of ring-core fibers for OAM transmission studies," *Opt. Express*, vol. 23, no. 8, pp. 10553–10563, Apr. 2015.
[11] P. Gregg, P. Kristensen, and S. Ramachandran, "Conservation of orbital angular momentum in air-core optical fibers," *Optica*, vol. 2, no. 3, p. 267, Mar. 2015.
[12] C. Brunet, P. Vaity, Y. Messaddeq, S. LaRochelle, and L. A. Rusch, "Design, fabrication and validation of an OAM fiber supporting 36 states.," *Opt. Express*, vol. 22, no. 21, pp. 26117–27, Oct. 2014.
[13] S. Ramachandran, J. W. Nicholson, S. Ghalmi, M. F. Yan, P. Wisk, E. Monberg, and F. V. Dimarcello, "Light propagation with ultralarge modal areas in optical fibers," *Opt. Lett.*, vol. 31, no. 12, p. 1797, Jun. 2006.
[14] N. Ahmed, K. M. Birnbaum, B. I. Erkmen, S. Dolinar, M. Tur, and A. E. Willner, "Mode Properties and Propagation Effects of Optical Orbital Angular Momentum (OAM) Modes in a Ring Fiber," *IEEE Photonics J.*, vol. 4, no. 2, pp. 535–543, Apr. 2012.
[15] C. Antonelli, A. Mecozzi, M. Shtaif, and P. J. Winzer, "Stokes-space analysis of modal dispersion in fibers with multiple mode transmission.," *Opt. Express*, vol. 20, no. 11, pp. 11718–33, May 2012.
[16] L. Wang, P. Vaity, Y. Messaddeq, L. Rusch, and S. Larochelle, "Orbital-Angular-Momentum Polarization Mode Dispersion in Optical Fibers and Its Measurement Technique," in *European Conference and Exhibition on Optical Communication*, 2015, p. Tu.3.3.4.
[17] F. Gori, "Polarization basis for vortex beams," *J. Opt. Soc. Am. A*, vol. 18, no. 7, p. 1612, Jul. 2001.
[18] L. Wang, P. Vaity, B. Ung, Y. Messaddeq, L. A. Rusch, and S. LaRochelle, "Characterization of OAM fibers using fiber Bragg gratings.," *Opt. Express*, vol. 22, no. 13, pp. 15653–61, Jun. 2014.
[19] J. P. Gordon and H. Kogelnik, "PMD fundamentals: Polarization mode dispersion in optical fibers," *Proc. Natl. Acad. Sci.*, vol. 97, no. 9, pp. 4541–4550, Apr. 2000.
[20] G. Milione, H. I. Sztul, D. A. Nolan, and R. R. Alfano, "Higher-Order Poincaré Sphere, Stokes Parameters, and the Angular Momentum of Light," *Phys. Rev. Lett.*, vol. 107, no. 5, p. 053601, Jul. 2011.
[21] C. R. Menyuk and P. K. A. Wai, "Polarization evolution and dispersion in fibers with spatially varying birefringence," *J. Opt. Soc. Am. B*, vol. 11, no. 7, p. 1288, Jul. 1994.
[22] P. K. A. Wai and C. R. Menyuk, "Polarization decorrelation in optical fibers with randomly varying birefringence," *Opt. Lett.*, vol. 19, no. 19, p. 1517, Oct. 1994.
[23] P. K. A. Wai and C. R. Menyuk, "Anisotropic diffusion of the state of polarization in optical fibers with randomly varying birefringence," *Opt. Lett.*, vol. 20, no. 24, p. 2493, Dec. 1995.
[24] J. N. Damask, *Polarization Optics in Telecommunications*, vol. 19. Springer Science & Business Media, 2004.
[25] C. D. Poole and D. L. Favin, "Polarization-mode dispersion measurements based on transmission spectra through a polarizer," *J. Light. Technol.*, vol. 12, no. 6, pp. 917–929, Jun. 1994.
[26] P. A. Williams and C. M. Wang, "Corrections to Fixed Analyzer Measurements of Polarization Mode Dispersion," *J. Light. Technol.*, vol. 16, no. 4, p. 534, Apr. 1998.
[27] C. Brunet, B. Ung, L. Wang, Y. Messaddeq, S. LaRochelle, and L. A. Rusch, "Design of a family of ring-core fibers for OAM transmission studies," *Opt. Express*, vol. 23, no. 8, pp. 10553–10563, 2015.
[28] B. Huttner, J. Reecht, N. Gisin, R. Passy, and J. P. Von der Weid, "Local birefringence measurements in single-mode fibers with coherent optical frequency-domain reflectometry," *IEEE Photonics Technol. Lett.*, vol. 10, no. 10, pp. 1458–1460, Oct. 1998.
[29] D. A. Nolan, X. Chen, and M.-J. Li, "Fibers With Low Polarization-Mode Dispersion," *J. Light. Technol.*, vol. 22, no. 4, p. 1066, Apr. 2004.

Lixian Wang received the Bachelor's degree in Microelectronics from Jilin University, Changchun, China, in 2006, and the Ph.D. degree in Physical Electronics from Institute of Semiconductors, Chinese Academy of Sciences, Beijing, China, in 2011. From 2011 to 2013 he was an assistant professor in Institute of Semiconductors, Chinese Academy of Sciences, where he worked on Microwave Photonics. He is currently a postdoctoral fellow in Centre d'optique, photonique et lasers (COPL), Université Laval, Québec, QC, Canada. His current research interests include spatial division multiplexing, fiber-based active and passive components such as fiber Bragg gratings and fiber lasers, and all optical signal processing.

Pravin Vaity received a Master's degree in physics from Mumbai University, India, in 2006 and a PhD degree in physics from Mohanlal Sukhadia University, Udaipur, India, in 2012. He was a research fellow from 2007 to 2012 as well a post-doctoral fellow from 2012 to 2013 at the Physical Research Laboratory, Ahmedabad, India. He also worked as a post-doctoral fellow in the Centre d'optique, photonique et lasers, Université Laval, Canada from 2013 to 2015. Currently, he is working as a post-doctoral associate at University of Notre Dame, United States. His research interests include optical vortices, orbital angular momentum modes in fiber, non-linear optics and photonic crystals.

Stéphane Chatigny holds a Master Degree in DWDM optical telecommunication from Laval University. From 1996 to 2000 at the National Optics Institute of Quebec City, he was involved in biophotonics research projects and military/civilian night vision systems development. In 2000-2001, he was successively at ITF optical and Access Photonic Networks, where he was involved in the development of components and systems for long haul, metro and access optical telecommunication networks. Since 2001, he works for CorActive where he is in charge of the development of chalcogenide fibers and specialty fibers at 1, 1.5 and 2µm for military, medical, industrial and telecommunication applications. He has authored more than 20 publications in international industry journals and holds 6 patents.

Younés Messaddeq received the Ph.D. degree in solid state chemistry in 1990 and the Bachelor's degree in solid state chemistry from the Université de Rennes 1, France, is one of the worlds most accomplished researchers in materials

development for optics and photonics. In his academic research, he has published more than 331 papers in referred journals and conferences, and presented several invited talks. His H-index is 35, and has well more than 4600 citations of his published works. In 2010, he was appointed to one of the 19 prestigious Canada Excellence Research Chairs, providing 28*M* in research funds at Université Laval, QC, Canada. He has been a Visiting Professor at the Physics Institute of So Carlos, Brazil; the Université de Bourgogne, France; and the University of Münster, Germany. He has also served as a Visiting Researcher and a Fellow at the National Institute for Inorganic Materials, Tsukuba, Japan. He has reported on his work in high-impact international publications.

Leslie Ann Rusch (S'91-M'94-SM'00-F'10) received the B.S.E.E degree (Hons.) from the California Institute of Technology, Pasadena, CA, USA, in 1980 and then the M.A. and Ph.D. degrees in electrical engineering from Princeton University, Princeton, NJ, USA in 1992 and 1994, respectively. She has experience in defense, industrial and academic communications research. She was a Communications Project Engineer for the Department of Defense from 1980–1990. While on leave from Université Laval, she spent two years (2001–2002) at Intel Corporation creating and managing a group researching new wireless technologies. She is currently a Professor in the Department of Electrical and Computer Engineering, Universit´e Laval, QC, Canada, performing research on wireless and optical communications. Her research interests include digital signal processing for coherent detection in optical communications, spatial multiplexing using orbital angular momentum modes in fiber, radio over fiber and OFDM for passive optical networks; and in wireless communications, optimization of the optical/wireless interface in emerging cloud-based computing networks, optical pulse shaping for high-bit rate ultrawide-band (UWB) systems, and implantable medical sensors with high bit rate UWB telemetry. She received the IEEE Canada J. M. Ham Award for Graduate Supervision. She has published more than 100 journal articles in international journals (90% IEEE/IEE) with wide readership, and contributed to more than 130 conferences. Her articles have been cited more than 3600 times per Google Scholar.

Sophie LaRochelle (M'00) received the Bachelor's degree in engineering physics from Université Laval, QC, Canada, in 1987, and the Ph.D. degree in optics from the University of Arizona, AZ, USA, in 1992. From 1992 to 1996, she was a Research Scientist at the Defense Research and Development Canada—Valcartier, where she worked on electrooptical systems. She is currently a Professor at the Department of Electrical and Computer Engineering, Université Laval, where she holds a Canada Research Chair (Tier 1) in Advanced Photonics Technologies for Emerging Communication Strategies. Her current research activities include active and passive components for optical communication systems including Bragg gratings filters, optical amplifiers, silicon photonic devices, multiwavelength, and pulsed lasers. Other research interests include spatial division multiplexing, all-optical signal processing and routing, and transmission of radio-over-fiber signals including UWB and GPS. She is a Senior Member of IEEE and a Fellow of OSA.